

Experimentally-Based Ocean Acoustic Propagation and Coherence Studies

Timothy F. Duda
Applied Ocean Physics and Engineering Department, MS 11
Woods Hole Oceanographic Institution
Woods Hole, MA 02543
phone: (508) 289-2495 fax: (508) 457-2194 email: tduda@whoi.edu

Award Number: N00014-11-1-0194
<http://www.whoi.edu/profile/tduda>

LONG TERM GOALS

The long-term goal is to better understand fluctuating sound propagation in two distinct ocean acoustic regimes: Stratified shallow water, where sound is highly bottom interacting, and the temperate deep-ocean sound channel. Acoustic field fluctuations have time scales varying from less than a minute to hours, and horizontal spatial scales from tens of meters to kilometers, comparable to processing time scales and system spatial scales, and thus impact exploitation of underwater sound. With proper understanding, reliable predictions of temporal and spatial variability of received underwater sound may be possible, thus improving processing and handling of signals of interest. Processing could include remediation of signal degradation and exploitation of available sonic information.

OBJECTIVES

An objective is to explain underwater sound fluctuation behavior that has been observed in both shallow and deep regimes. For shallow water, we seek to understand the mean and variability of transmission loss and phase at frequencies from 50 to 3000 Hz. For the deep-ocean sound channel, the objective is to better characterize coupled-mode propagation at 50 to 100 Hz over 100's to 1000's of kilometers. Propagation and forward scattering models, theoretical and computational, will be used to generate and to test hypotheses. Therefore, making better models is a second (enabling) objective.

APPROACH

The planned approach for the three-year project includes analysis of acoustic propagation variability signatures in preexisting datasets and comparison of these signatures with expectations derived from theory and models. Part of the final year will be dedicated to the planning of a potential future experiment to address questions that remain unanswered by this effort.

Data from multiple recent field exercises have been analyzed. For shallow water studies, data are mainly from the recent ONR Shallow-Water 2006 experiment (SW06, Figure 1) (Tang *et al.*, 2007). Additional shallow-water data are from the ASIAEX study (Chiu *et al.*, 2004; Duda *et al.*, 2004), the northeastern South China Sea spring 2007 ONR/Taiwan NLIWI acoustics experiment (Reeder *et al.*, 2010), the 1996/97 Shelfbreak PRIMER study (Lynch *et al.*, 2003), and the 2009 Quantifying,

Predicting and Exploiting Uncertainty study (QPE) (Gawarkiewicz *et al.*, 2011). The data for the deep-water studies are from the 2004 ONR Long-range Ocean Acoustic Propagation Experiment (LOAPEX) (Mercer *et al.*, 2009).

Planned activities are to continue analysis of these data sets, to compare the field data to theory and simulations, to improve the simulation capability, and to update theories, all with a focus on 3D effects. All of the shallow-water data sets are from stratified areas that support short-wavelength, high-frequency nonlinear internal waves and wave packets. We have quantified many first-order acoustic effects from these waves over the last decade or so. Because many of the effects are not described by two-dimensional (2D) environmental models or 2D acoustic models, our methods include fully 3D theories and fully 3D acoustic propagation simulations.

In each shallow-water field study, moored acoustic sources transmitted signals to moored acoustic receivers, and large numbers of other sensors measured environmental variations. Temporal variations of the acoustic propagation conditions were examined and compared directly with local conditions and with data-driven predictions.

In the deep-water study, sound was transmitted from ship-lowered sources to vertical line arrays moored north of Hawaii in the North Pacific. The source-to-receiver distances were 50 to 3200 km (Figure 2). The deep-water studies under this grant are led by Dr. Ilya Udovychenkov.

WORK COMPLETED

A large number of LEAR/SW06 pulses transmitted from moored sources to the WHOI L-array (co-located HLA/VLA) have been analyzed. A journal article appeared this year describing the spatial coherence of 100 to 400 Hz acoustic signals measured with the horizontal line array (HLA) portion of the L-array resting on the seafloor at 80 m depth (Duda *et al.*, 2012). Figure 1 shows the experimental arrangement. The HLA was 32 channels, 465 m long, on a north-south line.

That article required the largest amount of SW06 analysis on our part. Additional SW06-related work by us contributed (with authorship) to four other acoustics publications. Density-compensated temperature and salinity contributions to sound speed anomalies observed in the field were carefully analyzed, pushing the measurement capability of our systems (Colosi *et al.*, 2012a). A coupled-mode propagation model, calibrated with field-observed sound-speed profiles, was used to predict mean intensity and mean-squared intensity in shallow-water conditions of small random internal waves, away from very large internal waves (Colosi *et al.*, 2012b). Note that this is a different situation from our other studies of sound propagation within very strong internal wave “coherent structures”. One of the other papers covers propagation anomalies of this type, in straight and curved large internal waves (McMahon *et al.*, 2012). The fourth paper of this group involves analysis of azimuthal intensity dependence of order-900 Hz signals transmitted 7.5 km, in various directions, in the presence of anisotropic strong internal waves (Lynch *et al.*, 2012).

In addition to the SW06 acoustics work, the PI was coauthor of two publications concerning internal tide predictability in the SW06 region (Nash *et al.*, 2012a, Nash *et al.*, 2012b). The study of internal tides, and the nonlinear internal wave packets they spawn, is crucial to understanding acoustic propagation behavior in the outer continental shelf environment. Therefore this work is closely tied into the goal of understanding acoustic effects in the real ocean.

Characterization of internal tides and internal waves was also done in support of the QPE study. This work has resulted in a submitted journal article. Figure 3 shows the work area. The figure also shows an example of the nonlinear internal waves that were characterized in the region. The echo sounder and radar data were combined to determine wavelength, wave speed, and wave amplitude enough to allow quantitative comparison with strongly nonlinear waves modeled with Long's Equation. The figure shows that this model can describe these waves, and can be used to determine wave energy. The figure also demonstrates (again) that the echo sounder is a useful tool in this region for this type of work.

The study of LOAPEX acoustic arrivals at 50 to 3200 km distance in the North Pacific (Figure 2) has resulted in a comprehensive paper on the subject of deep-ocean low-order mode dispersion (Udovydchenkov *et al.*, 2012a). This is a primary LOAPEX study topic. The spreading in time of mode-filtered sound arrivals (intended to quantify arrivals of energy contained in individual acoustic normal modes) agrees with predictions for a sound source near the depth of the sound speed minimum. The degree of agreement is sensitive to details used in the prediction, such as environmental mismatch. In addition, the LOAPEX work has resulted in two other publications this year. The first involves unified processing of acoustic data from two VLAs separated by a few km (Udovydchenkov *et al.*, 2012b). The second contains an analysis of seafloor reflecting sound at 50-km range (Udovydchenkov *et al.*, 2012c). At this range, the reflected sound interferes with non-reflected sound, and it also contains potentially useful information about seafloor geoacoustic properties.

RESULTS

SW06/LEAR: The publication of the full analysis of the SW06 L-array fluctuation data set (Duda *et al.*, 2012) validates some of our earlier findings (Collis *et al.*, 2008). Horizontal array gains and coherence lengths L_d for along-internal wave duct propagation and for across-internal wave duct propagation were highly variable for the entire experiment. An appendix of the paper shows the relationship between the broadband correlation function that we analyzed, which is useful for pulses, and the traditional narrowband correlation function.

The results show both rapid variability and slow trends of coherence length and array gain. Figure 4 shows time series of short-term mean values (24-hr and 3-hr windows) of signal coherence length, obtained with a broadband method. The coherence lengths are defined as e-folding scales of spatially lagged covariance functions of complex demodulated signals. The phase variation governs the decorrelation, not the intensity, found by phase-structure function analysis and analysis of intensity. Figure 5 shows horizontal array gain and array gain degradation (AGD) variations between two 2.4-hour windows of the experiment for two different array aperture sizes. The array gain is defined as the signal to noise ratio for coherently added (beam steered) acoustic receptions with an array, divided by the signal to noise ratio for a single array element. AGD is theoretical array gain minus achieved gain (all in dB), so that for an M -element array $AGD.M = 10(\log_{10}M - \log_{10}G)$, where gain G is defined as the signal power to noise power ratio for the coherent sum divided by the same ratio for a single element. Figure also shows G versus beam steering heading for different apertures.

Figure 4 shows that coherence behavior was strongly anisotropic. Along internal wave-crest and across wave crest sound propagation differs in temporal variability of L_d and mean L_d . Sound from the 30-distant NW sources (Figure 1) traveling in the same direction as internal waves (across crest) showed steady short L_d , approximately 10 to 15 acoustic wavelengths for both 224 and 400 Hz. Sound from 19-km distant NE sources at 100 and 200 Hz traveling perpendicular to the internal-wave propagation

direction along crests) had highly variable L_d for short processing windows of 3 h. As internal waves passed, L_d dropped from ~ 25 to ~ 7 wavelengths at 100 Hz, and from ~ 40 to ~ 7 wavelengths at 200 Hz. Figure 6 shows time-dependent coherence behavior. Figure 7 shows how coherence length and beam deflection they are related, in a scatter plot.

Continuing with SW06, (Colosi *et al.*, 2012a) describes the nature of sound-speed variability from density compensated temperature and salinity fluctuations along isopycnals (so-called spiciness), and quantifies the internal-wave normal modal bandwidth (mode spectrum). Another paper investigates cross coherence of acoustic normal modes in low-frequency shallow-water propagation, yielding apparently robust estimates of mean acoustic fields in fluctuating conditions and range evolution of the scintillation index (Colosi *et al.*, 2012a).

QPE: Fishing activity made measurements with moored instruments almost impossible in this area. Only trawl-proof ADCP's on the seabed were sensible for extended periods. The submitted journal article shows that we were able to gain useful information about larger internal waves in this region using the echo sounder and the radar on the research vessel, not previously done with this particular instrument suite. The data allowed quantitative modeling of the internal waves, to better characterize them, and to show which level of nonlinear wave model was needed to describe the wave physics. Internal tides in the region were also quantified in the paper and compared to those of other regions.

LOAPEX: The temporal structure of measured modal group arrivals (modal pulse width) was compared to theoretical predictions and numerical simulations. Theory, simulations, and observations generally agree (Udovychenkov *et al.*, 2012a). For situations having poor agreement, reasons for the disagreement have been analyzed in terms of the underlying physical processes and data limitations. Recent work on bottom-interacting sound recorded at 50-km range shows some promise for separation of bottom-reflecting and direct energy and for seafloor geoacoustic property inversion, shown in Figure 8 (Udovychenkov *et al.*, 2012c).

IMPACT/APPLICATIONS

The results may be useful for guiding coherent signal processing, particularly of horizontal array data. There is a potential for algorithms that are robust to signal fluctuations, or which may exploit them.

RELATED PROJECTS

The PI collaborates with Dr. Y.-T. Lin of WHOI on computational efforts. The PI is working with other ONR PI's analyzing data from the SW06, 2007 South China Sea, and ONR QPE experiment sites. The PI also has another project in its second year, Integrated Ocean Dynamics and Acoustics (IODA), a DoD MURI project, administered by this ONR code, intended to improve acoustic modeling and prediction by coupling improved acoustic models to improved high-resolution ocean environmental models.

REFERENCES

Chiu, C.-S., S. R. Ramp, C. W. Miller, J. F. Lynch, T. F. Duda, and T. Y. Tang, Acoustic intensity fluctuations induced by South China Sea internal tides and solitons, *IEEE J. Oceanic Eng.*, 29, 1249-1263, 2004.

- Collis, J. M., T. F. Duda, J. F. Lynch, and H. A. DeFerrari, Observed limiting cases of horizontal field coherence and array performance in a time-varying internal wavefield, *J. Acoust. Soc. Am.* 124, EL97-EL103, 2008.
- Duda, T. F., J. F. Lynch, A. E. Newhall, L. Wu, and C.-S. Chiu, Fluctuation of 400-Hz sound intensity in the 2001 ASIAEX South China Sea Experiment, *IEEE J. Oceanic Eng.*, 29, 1264-1279, 2004.
- Gawarkiewicz, G., S. Jan, P. F. J. Lermusiaux, J. L. McClean, L. Centurioni, K. Taylor, B. Cornuelle, T. F. Duda, J. Wang, Y. J. Yang, T. Sanford, R.-C. Lien, C. Lee, M.-A. Lee, W. Leslie, P. J. Haley Jr., P. P. Niiler, G. Gopalakrishnan, P. Velez-Belchi, D.-K. Lee, and Y. Y. Kim, Circulation and intrusions northeast of Taiwan: Chasing and predicting uncertainty in the cold dome, *Oceanography*, 24, 110-121, doi: 10.5670/oceanog.2011.99, 2011.
- Lynch, J.F., A.E. Newhall, B. Sperry, G.G. Gawarkiewicz, A. Fredricks, P.L. Tyack, C.-S. Chiu, and P. Abbot, Spatial and Temporal Variations in Acoustic Propagation Characteristics at the New England Shelfbreak Front, *IEEE J. Ocean. Eng.*, 28, 129-150, 2003.
- Mercer, J. A., J. A. Colosi, B. M. Howe, M. A. Dzieciuch, R. Stephen, and P. F. Worcester, LOAPEX: The Long-Range Ocean Acoustic Propagation Experiment, *IEEE J. Oceanic Eng.*, 34, 1-11, 2009.
- Reeder, D. B., L. Y. S. Chiu, and C.-F. Chen, Experimental evidence of horizontal refraction by nonlinear internal waves of elevation in shallow water in the South China Sea: 3D vs. Nx2D acoustic propagation modeling, *J. Comput. Acoust.*, 18, 267–278, 2010.
- Tang, D. J., J.N. Moum, J.F. Lynch, P. Abbot, R. Chapman, P. Dahl, T. Duda, G. Gawarkiewicz, S. Glenn, J.A. Goff, H. Graber, J. Kemp, A. Maffei, J. Nash and A. Newhall, ShallowWater 2006: a joint acoustic propagation/nonlinear internal wave physics experiment, *Oceanography*, 20(4), 156-167, 2007.

PUBLICATIONS

- Chiu, Linus Y.-S., Ying-Tsong Lin, Chi-Fang Chen, Timothy Duda, and Brian Calder, Focused sound from three-dimensional sound propagation effects over a submarine canyon. *J. Acoust. Soc. Am. Express Letters*, 129, EL260-EL266, 2011. [published, refereed]
- Colosi, J. A., T. F. Duda, Y.-T. Lin, J. F. Lynch, A. E. Newhall, and B. D. Cornuelle, Observations of sound-speed fluctuations on the New Jersey continental shelf in the summer of 2006, *J. Acoust. Soc. Am.*, 131, 1733-1748, 2012a. [Published, refereed]
- Colosi, J. A., T. F. Duda, and A. K. Morozov, Statistics of low-frequency normal-mode amplitudes in an ocean with random sound-speed perturbations: Shallow water environments, *J. Acoust. Soc. Am.*, 131, 1749-1761, 2012b. [Published, refereed]
- Duda, T. F., Y.-T. Lin and D. B Reeder, Observationally-constrained modeling of sound in curved ocean internal waves: Examination of deep ducting and surface ducting at short range, *J. Acoust. Soc. Am.*, 130, 1173-1187, 2011a. [Published, refereed]
- Duda, T. F., Y.-T. Lin, W. Zhang, B. D. Cornuelle and P. F. J. Lermusiaux, Computational studies of three-dimensional ocean sound fields in areas of complex seafloor topography and active ocean dynamics, in *Proceedings of the 10th International Conference on Theoretical and Computational Acoustics*, Taipei, Taiwan, 2011b. [published, not refereed]

- Duda, T. F., Theory and observation of anisotropic and episodic internal wave effects on 100-400 Hz sound, in Proceedings of the International Conference and Exhibition on Underwater Acoustic Measurements: Technologies and Results, Kos, Greece, pp. 999-1006, 2011. [published, not refereed]
- Duda, T. F., J. M. Collis, Y.-T. Lin, A. E. Newhall, J. F. Lynch, and H. A. DeFerrari, Horizontal coherence of low-frequency fixed-path sound in a continental shelf region with internal-wave activity, *J. Acoust. Soc. Am.*, 131, 1782-1797, 2012. [Published, refereed]
- Gawarkiewicz, G., S. Jan, P. F. J. Lermusiaux, J. L. McClean, L. Centurioni, K. Taylor, B. Cornuelle, T. F. Duda, J. Wang, Y. J. Yang, T. Sanford, R.-C. Lien, C. Lee, M.-A. Lee, W. Leslie, P. J. Haley Jr., P. P. Niiler, G. Gopalakrishnan, P. Velez-Belchi, D.-K. Lee, and Y. Y. Kim, Circulation and intrusions northeast of Taiwan: Chasing and predicting uncertainty in the cold dome, *Oceanography*, 24, 110-121, doi: 10.5670/oceanog.2011.99, 2011. [Published, refereed]
- Lin, Y.-T., A. E. Newhall, T. F. Duda and C.-F. Chen, Numerical Considerations For Three-Dimensional Sound Propagation Modeling: Coordinate Systems And Grid Sizes, in Proceedings of the 10th International Conference on Theoretical and Computational Acoustics, Taipei, Taiwan, 2011. [published, not refereed]
- Lynch, J. F., C. Emerson, P. A. Abbot, G. G. Gawarkiewicz, A. E. Newhall, Y.-T. Lin, and T. F. Duda, On whether azimuthal isotropy and alongshore translational invariance are present in low-frequency acoustic propagation along the New Jersey shelfbreak, *J. Acoust. Soc. Am.*, 131, 1762-1781, 2012. [Published, refereed]
- McMahon, K. G., L. K. Reilly-Raska, W. L. Siegmann, J. F. Lynch, and T. F. Duda, Horizontal Lloyd mirror patterns from straight and curved nonlinear internal waves, *J. Acoust. Soc. Am.*, 131, 1689-1700, 2012. [Published, refereed]
- Nash, J., S. Kelly, E. Shroyer, J. Moum, and T. Duda, The unpredictability of internal tides in coastal seas. In Proc. 7th International Symposium on Stratified Flows, Rome, Italy, 2011. [published, not refereed]
- Nash, J. D., E. L. Shroyer, S. M. Kelly, M. E. Inall, T. F. Duda, M. D. Levine, N. L. Jones, and R. C. Musgrave, Are any coastal internal tides predictable? *Oceanography*, 25, 80-95, 2012a. [Published, refereed]
- Nash, J. D., S. M. Kelly, E. L. Shroyer, J. N. Moum, and T. F. Duda, The unpredictable nature of internal tides on the continental shelf, *J. Phys. Oceanogr*, in press, 2012b. <http://dx.doi.org/10.1175/JPO-D-12-028.1> [In press, refereed]
- Udovydchenkov, I. A., M. G. Brown, T. F. Duda, J. A. Mercer, R. K. Andrew, P. F. Worcester, M. A. Dzieciuch, B. M. Howe, and J. A. Colosi, Modal analysis of the range evolution of broadband wavefields in the North Pacific Ocean: Low mode numbers, *J. Acoust. Soc. Am.*, 131, 4409-4427, 2012a. [Published, refereed]
- Udovydchenkov, I. A., M. G. Brown, and T. F. Duda, Piecewise coherent mode processing of acoustic data recorded on two horizontally separated vertical line arrays, *J. Acoust. Soc. Am.*, 131, EL492-498, 2012b. [Published, refereed]
- Udovydchenkov, I. A., R. A. Stephen, T. F. Duda, S. T. Bolmer, P. F. Worcester, M. A. Dzieciuch, J. A. Mercer, R. K. Andrew, and B. M. Howe, Bottom interacting sound at 50 km range in a deep ocean environment, *J. Acoust. Soc. Am.*, 132, 2224-2231, 2012c. [Published, refereed]

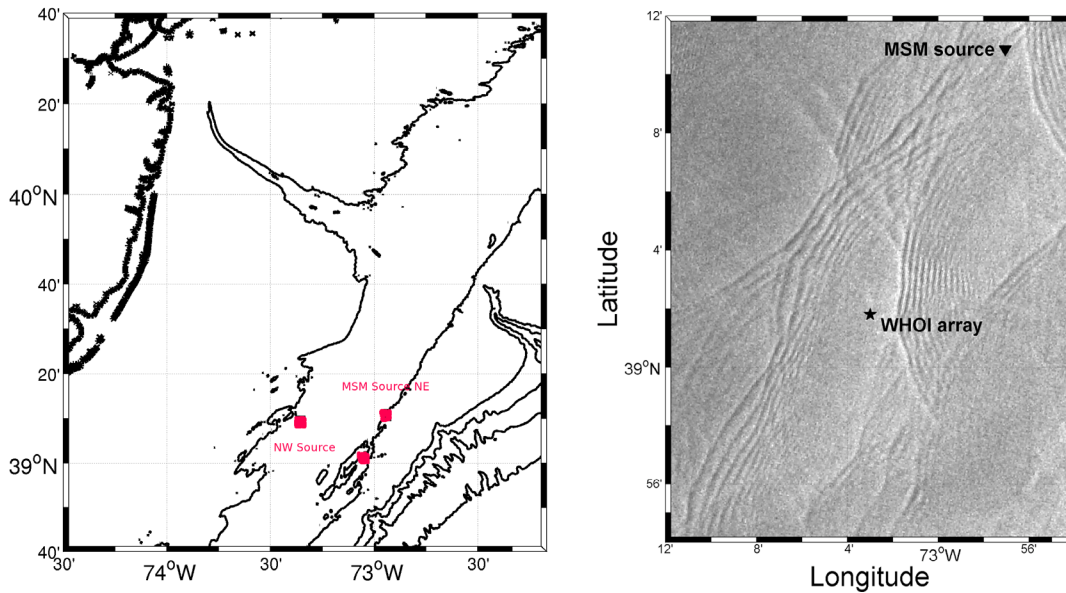


FIG. 1. (left) The SW06 site is shown. New York harbor is at the extreme upper left corner. Contours at 0 m (coastline, thick line), 50, 80, 200, 500, 1000 and 2000 m are shown, with the 80-m isobath crossing Hudson Canyon in a nearly straight line at 39-40 N, 72-30 W. Three squares show the WHOI L-array receiver (southernmost) at approximately 39-1 N, 73-3 W, the 'NE' acoustic source mooring position 19 km to the northeast, and the 'NW' source mooring position 32 km to the northwest. (right) A satellite SAR image showing internal wave surface signatures from the University of Miami (CSTARS) is shown, with two mooring positions repeated from the other frame.

[(left) The chart shows receiver and NE positions at 80-m contour, NW near the 50-m contour. Hudson Canyon is north and northeast of these. (right) Many internal wave packets traveling westward are seen in the image, with one to three waves per km and three to eight waves per packet.]

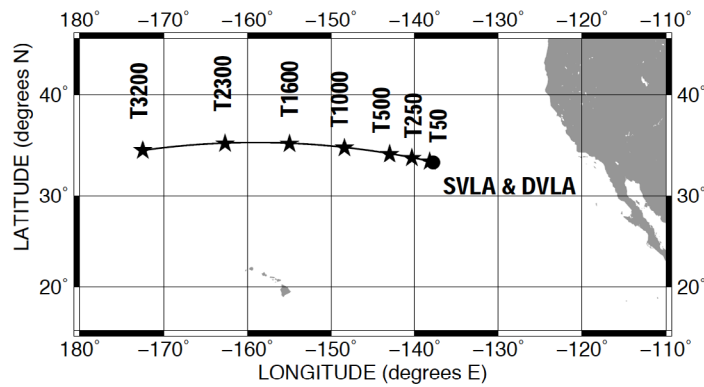


FIG. 2. *The geometry of the LOAPEX experiment in the eastern North Pacific Ocean is shown. Two vertical line arrays of hydrophones were deployed at the location denoted by SVLA and DVLA. The source was suspended from the ship at seven stations labeled T50, T250, ... , T3200 at one or more of these depths: 350 m, 500 m, and 800 m.*

[The receivers were near 33.4 N, 137.7 W, approximately 1500 km west of Los Angeles. The source stations were to the west along a geodesic, at distances of 50, 250, 500, 1000, 1600, 2300 and 3200 km. Station T3200 was near 34.6 N, 172.5 W.]

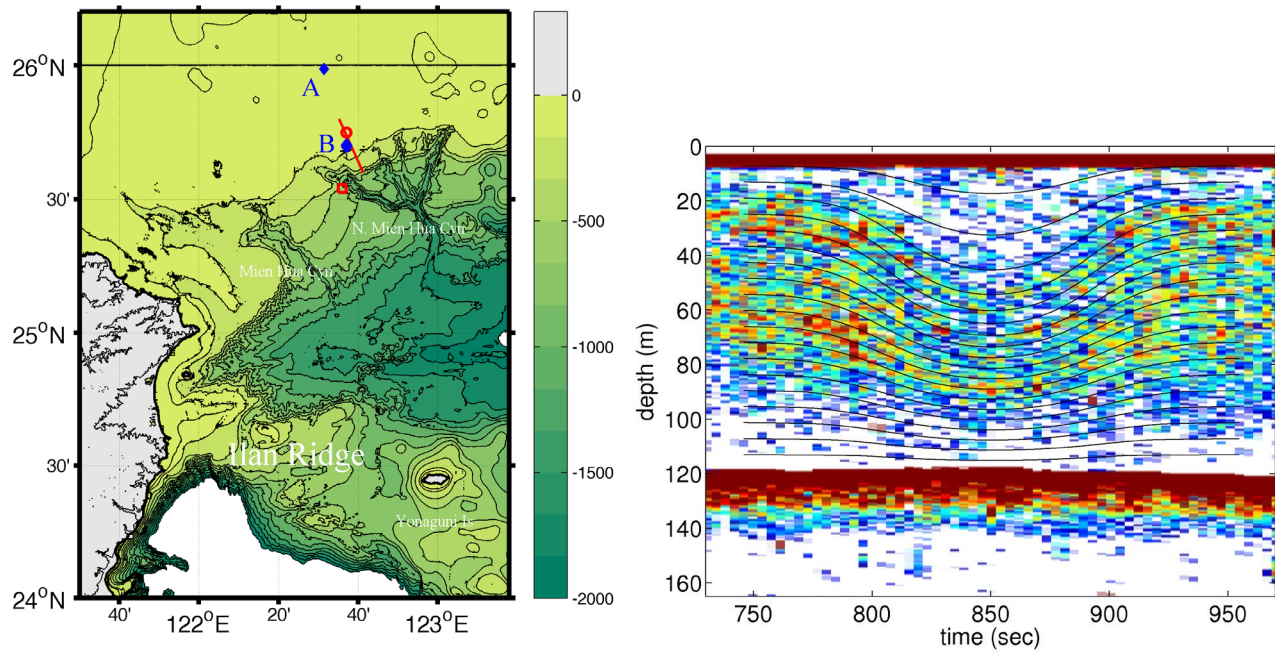


FIG 3. (left) A chart of the QPE study area is shown. Sites A and B (mooring areas) are marked with blue diamonds. Site B is a short distance north of the west branch of North Mien Hua Canyon. The depth contour interval is uniform at three per 500 m, with an additional 100-m contour added with no color change. The white area at the south is deeper than 2000 m. The line at 26°N is an artifact of a database change. (right) Scattering layers displaced by an internal wave are seen in the ship's EK500 echo sounder range-gated intensity plot, with red being highest intensity, white lowest. The black lines show streamlines of a highly nonlinear internal wave modeled to fit.

[A chart is shown on the left. Sites A and B are 75 km northeast of the northeast corner of Taiwan, in shallow water, with deep water to the south, and near the head of a canyon system. The right panel shows an internal wave of 30-m displacement in 120 m of water. The modeled wave fits the data well.]

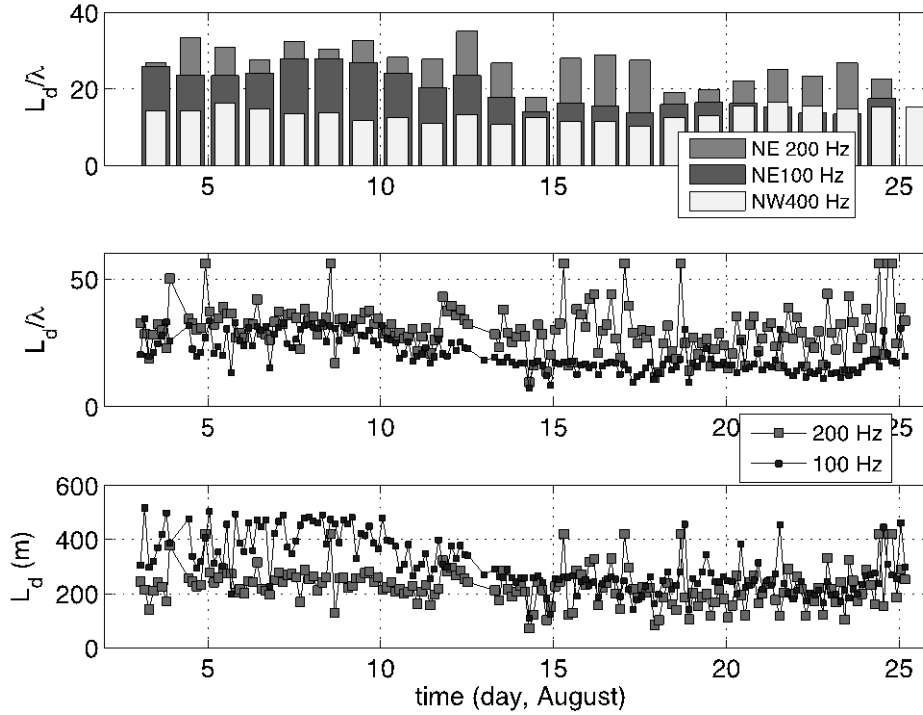


FIG. 4. (top) One-day average horizontal coherence scale, normalized using acoustic wavelength, measured at the HLA receiver, is plotted for three SW06 acoustic sources: NE 200 Hz, NE 100 Hz, and NW 400 Hz. (See Fig. 1 for positions.) (middle) Normalized horizontal coherence scales are shown for the two NE sources, with three-hr averaging in place of 24-hr averaging. (bottom) The results of the middle panel are shown again without normalization with respect to wavelength. From Duda et al., 2012.

[(top) NW 400 Hz coherence for a transmission path across internal-wave crests is shorter and steadier than the others, at 15 wavelengths. The others are 25 to 30 wavelengths for about ten days, then drop to 15-20 wavelengths for about ten days. (middle) The three-hour average results are near 30 wavelengths for ten days, then diverge for ten days to a steady value of 15 wavelengths for 100 Hz and a fluctuating higher value for 200 Hz. (bottom) The dimensional correlation lengths differ for the two frequencies over the first ten days, being greater for 100 Hz, and are similar for the two frequencies over the final ten days.]

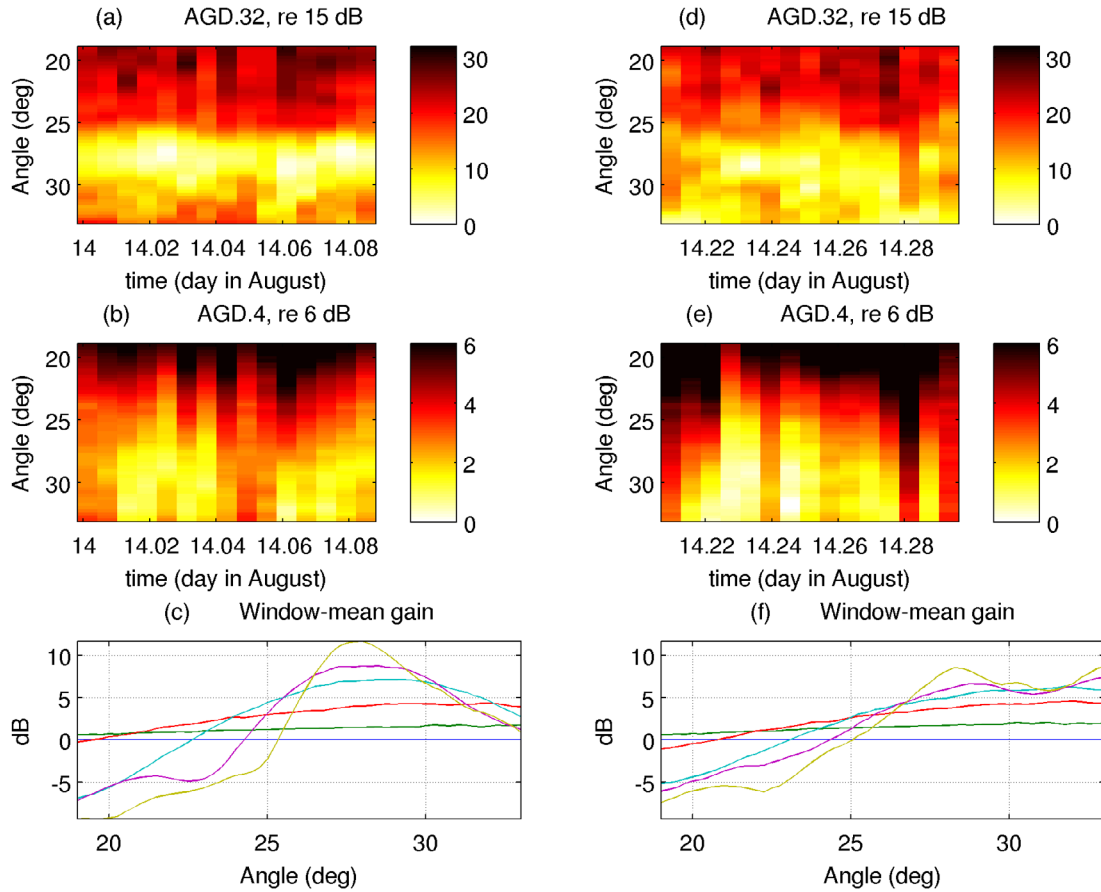


FIG. 5. 200-Hz (NE) array gain degradation (AGD) (a), (b), (d), (e) and array gain (c), (f) are shown, all in dB units. Results are from two 2.4-h long periods on 14 August, hours 0–2.4 [left, (a)–(c)] and hours 4.8–7.2 [right, (d)–(f)]. (a) and (d) show full-array AGD results (32 elements at 15-m spacing) for a fan of steering angles. White indicates zero array gain degradation (theoretical SNR gain of 15 dB achieved). (b) and (e) show four-element subarray results in a similar format as the 32-element results (theoretical gain is 6 dB). (c) and (f) show window-mean gain at each setting angle, converted to dB after averaging. Subarray sizes are one element (flat line, no gain), 2, 4, 8, 16, and 32 elements. The highest gain is achieved with 32 elements. The gain increases monotonically with subarray length near 28° for each window, indicating line coloration. The first period (left) has weak internal waves and one strong peak of high gain. The later period (right) has two lower gain peaks, suggesting horizontal acoustic multipath and interference. From Duda et al, 2012.

[The top four panels show lowest AGD meandering in angle over time for both time periods and both array sizes. The minimum AGD sometimes rises to 3 or 4 dB or greater. The left lowest panel (weak internal waves) shows higher gain than the right panel (strong internal waves), and also shows maximum gain in the steering direction toward the source. The right lowest shows lower gain and two peaks for 16 and 32 elements, at 28 and 32 degrees from north.]

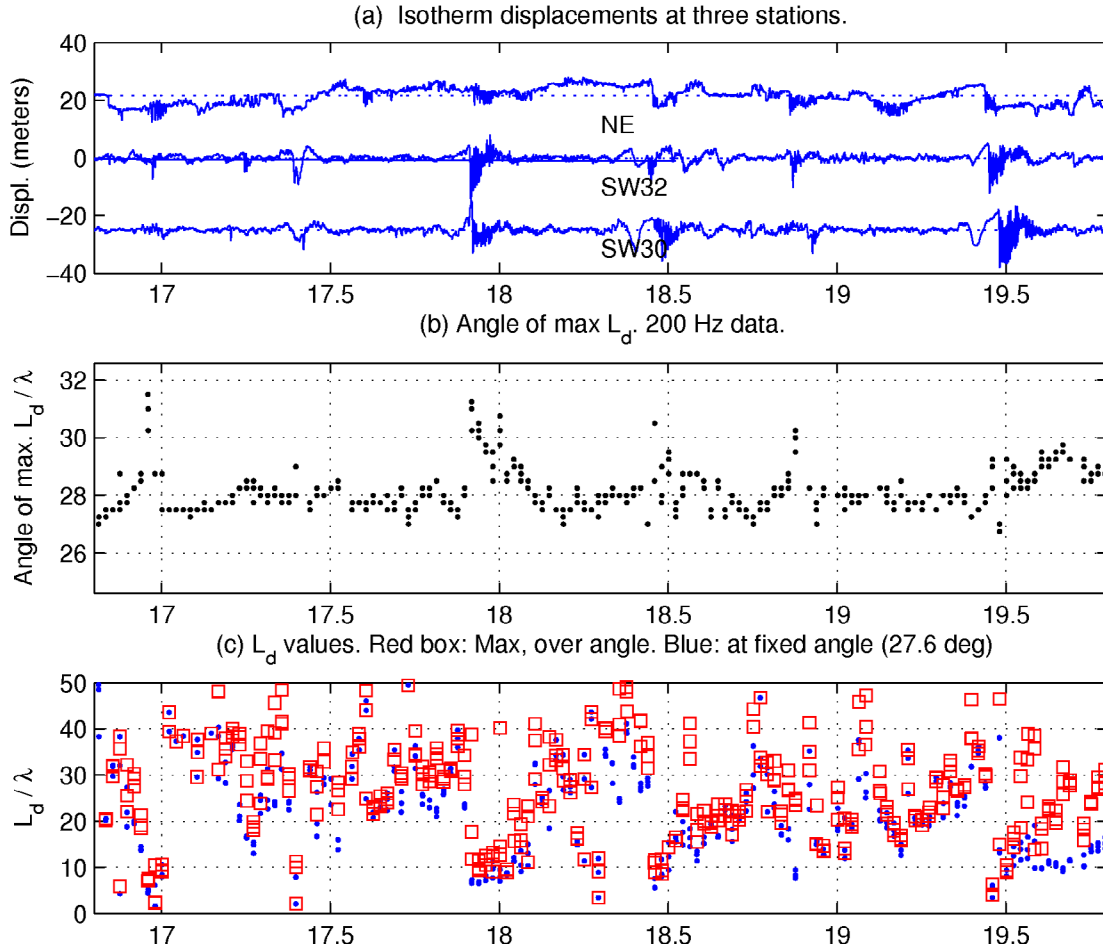


FIG 6. Wave and pulse parameters for the 200-Hz northeast source are shown for August 16-19, 2006. (a, top) Time series of thermocline displacements collected at moorings along the acoustic path, showing internal wave packets. The top trace is near the source, the middle trace is midway along the track, and the bottom trace is near the receiver. (b) The HLA steering angle with maximum horizontal field coherence length L_d is shown. (c) The coherence length L_d divided by the acoustic wavelength is plotted. The red dots show the maximum L_d as a function of time. The blue dots show L_d at the fixed angle of 28.2 degrees.

[During multiple intervals of strong internal waves the acoustic coherence parameters are altered, with beam angle changing from 28 to 31 degrees and coherence length falling from 50 to 7 wavelengths.]

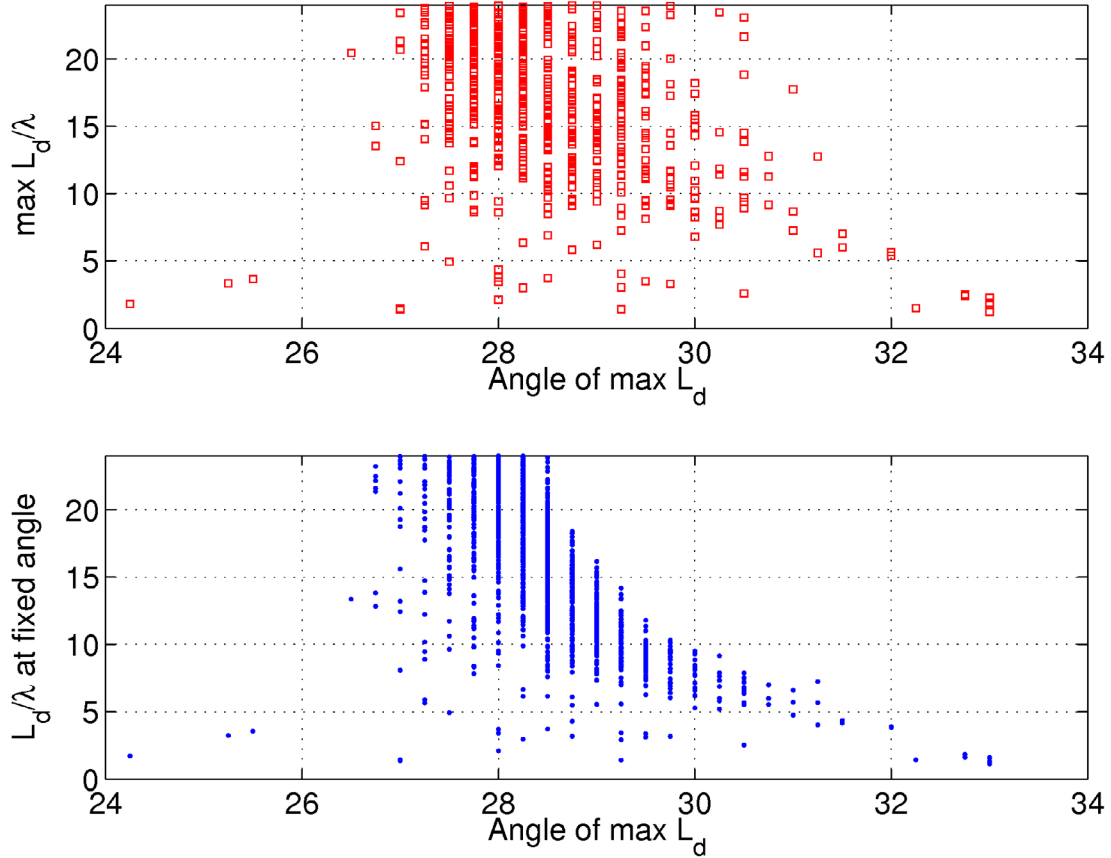


FIG 7. Three of the parameters shown in Figure 6 are plotted against one another. On the top, the maximum correlation length $\max(L_d/\lambda)$, where λ is acoustic wavelength, is plotted against the beam steering angle where this occurs. On the bottom, $\max(L_d/\lambda)$ is alternatively plotted against L_d/λ in the direction toward the sound source. The lower show a significant relation between the two parameters, interpreted as deflection (usually by internal waves) of an arriving waveform with a narrow coherent beam pattern. The somewhat uniform relationship on the top suggests that the maximum coherence of the arriving waveform is not statistically related to the beam deflection (consistent with statistical tests). The quantity of points in the plots is 3096, collected over 22.5 days.

[(top) For max coherence direction of 27 to 30 degrees the $\max(L_d/\lambda)$. can have any value from 2 to 20, or greater (the plot does not show high $\max(L_d/\lambda)$). Extreme values of maximum coherence direction 24 to 27 and 30 to 33 tend to have low $\max(L_d/\lambda)$. The result is no trend. (Bottom) a trend can be detected, with lower L_d/λ in the direction toward the sound source at higher angle of $\max(L_d/\lambda)$.]

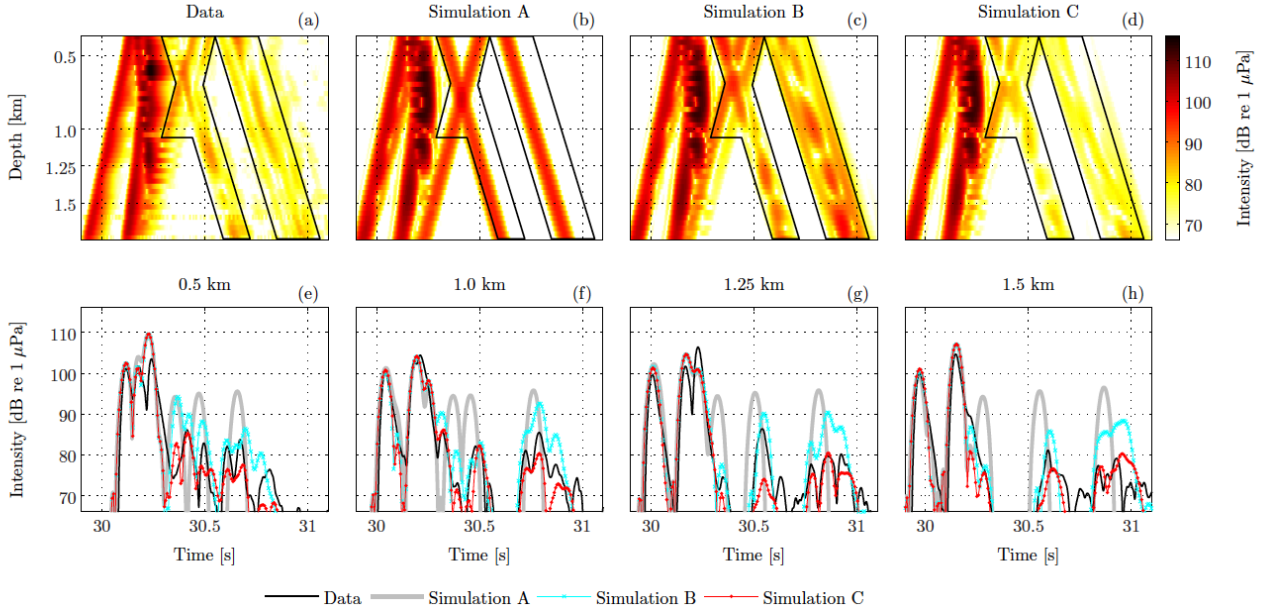


FIG. 8. (a) The observed wave field recorded during one of the five-minute LOAPEX transmissions from T50 with the source at 800 m depth is compared with simulations. The simulation scenarios are (b) flat topography and uniform bottom properties, (c) real topography and more realistic bottom properties, and (d) real topography with “best-fit” bottom properties. Black solid lines in the upper four panels outline the domain that includes most of the bottom-reflected energy. The lower four panels show data and model acoustic intensities at depths of 500, 1000, 1250, and 1500 m (panels (e)-(h) respectively). The mean relative misfit (defined in Udovydchenkov et al., 2012c) between the data and Simulation A is 10.8 ± 2.0 ; between the data and Simulation B is 4.8 ± 1.0 ; and between the data and Simulation C is 0.74 ± 0.06 . Figure from Udovydchenkov et al., 2012c.

[The Simulation C intensity as a function of depth and time, shown in (d), most closely matches the data in (a). The Simulation C waveforms also most closely match the data for the four plotted depths.]